Received: 30 November 2025 | Revised: 24 January 2026 | Accepted: 5 February 2026

DOI: 10.1002/aic.70294

AIChE JOURNAL

RESEARCH ARTICLE

Reaction Engineering, Kinetics and Catalysis

Improved symmetry and current distribution in a gastight rotating cylinder electrode cell: Design and characterization

Momoko Ishida[1] | Tyler Seung Hun Kwak[1] | Derek M. Richard[1] | Saudagar Dongare[2] | Burcu Gurkan[2] | Panagiotis D. Christofides[1] | Carlos G. Morales-Guio[1]

[1]Department of Chemical and Biomolecular Engineering, University of California, Los Angeles, California, USA

[2]Department of Chemical and Biomolecular Engineering, Case Western Reserve University, Cleveland, Ohio, USA

Correspondence
Carlos G. Morales-Guio, Department of Chemical and Biomolecular Engineering, University of California, Los Angeles, CA, USA.
Email: moralesguio@ucla.edu

Funding information
U.S. Department of Energy, Grant/Award Number: DE-SC0023427; National Science Foundation, Grant/Award Number: CBET-2339693

Abstract

Understanding the interplay between intrinsic kinetics and transport remains a central challenge in electrocatalysis. Rotating disk electrodes (RDE) are widely used because their transport can be described analytically, but radial concentration gradients complicate analysis of multi-electron processes. Rotating cylinder electrodes (RCE) provide an improved convective transport profile that better separates transport from kinetics. However, multiphysics simulations show that the use of a single flat counter electrode distorts the electric field in low-conductivity electrolytes. We present a third-generation gastight RCE cell (RCE-3) with two flat counter electrodes symmetrically positioned around the cylinder. This configuration doubles the counter electrode area, increases achievable current density, and improves field symmetry while maintaining well-defined hydrodynamics. Electrochemical CO_2 reduction experiments demonstrate that asymmetric electric fields bias apparent kinetics in non-aqueous electrolytes, whereas symmetric counter electrode operation minimizes these distortions, enabling reliable extraction of intrinsic kinetic parameters. The RCE-3 cell contributes to advancing the mechanistic understanding of non-aqueous electrocatalytic systems.

KEYWORDS
N/A

1 | INTRODUCTION

Electrochemical cells are the primary tools used to study electrocatalytic reactions. The three main components of these cells are the electrodes (anode and cathode), the electrolyte, and the vessel. The various designs of electrochemical cells offer different mass transport[1] and electric field profiles.[2] Glass and polymer vessels with one or two compartments have been traditionally employed in electrocatalysis because they are commercially available, easy to assemble, and require little specialized expertise for their operation, while still enabling reproducible characterization of catalyst performance within the same cell.[3] Among the most common electrode designs are rotating disk electrodes (RDE),[4] which allow systematic variation of mass transport resistance[5] by controlling the thickness of the concentration boundary layer through the electrode's rotation rate.[6] In recent years, electrochemical cell and electrode designs have become more diverse and correspondingly more complex in their assembly, operation, and mathematical description.[7] For example, gas diffusion electrodes (GDE) cells use thin porous catalyst layers deposited on gas diffusion layers that enhance mass transport compared to stagnant or mechanically stirred electrolytes.[8] While in RDE systems and stagnant electrochemical cells the concentration boundary layer ranges from tens to hundreds of micrometers in thickness, in GDEs the concentration boundary layer is reduced to only a few nanometers at the three-phase boundary.[9] Thin concentration boundary layers are particularly useful in the study of small gas molecule activation chemistries such as CO_2,

N_2, CO, CH_4, and $NO_x$where the reactant has a low solubility in the electrolyte. GDEs, however, have complicated three-dimensional and temporal concentration gradients that complicate the study of intrinsic reaction kinetics.[10] With growing interest in evaluating catalysts under conditions relevant to industrial operation, specialized vessel designs have also been introduced to probe the influence of temperature[11] and pressure.[12] However, these designs often neglect potential asymmetries in transport and electric fields, complicating the reliable extraction of intrinsic kinetic parameters and limiting the translation of catalytic performance and insights across different vessel and electrode geometries.[13] Understanding the relation between reactor kinetics (the result of the pairing of the electrodes with the vessel) and reaction kinetics (each electrode individually independent of the vessel) is a standing challenge in electrochemical engineering and requires the development and use of electrochemical cells with well-defined transport characteristics.[14]

Among electrochemical cells with well-defined and controllable hydrodynamics, the RDE has become the most widely adopted rotating geometry in electrocatalysis. The relation between hydrodynamics and mass transport is described analytically by the Levich equation, which connects the diffusion-limited current to electrode rotation speed, kinematic viscosity, and species diffusivity, providing a simple quantitative framework to separate mass transport from reaction kinetics.[15] However, the RDE geometry inherently produces radial concentration gradients across the disk surface,[5] which complicates the interpretation of potential-dependent kinetics for multi-electron processes.[16] These limitations are not present in the rotating cylinder electrode (RCE), where convective mass transport ensures the development of uniform secondary and ternary current distributions.[17] In contrast to the RDE, the RCE provides a uniform transport boundary layer across the electrode surface,[14] facilitating isolation of intrinsic kinetics. Despite these advantages, RCEs remain relatively uncommon in electrocatalysis, even though they are widely used in corrosion engineering[18] and metal protection research,[19] where accurate mass transport control is critical.

Until recently, RCE cells that were both gastight and compatible with rigorous electrocatalytic analysis were not available. The challenge lies in the dual requirement of hermetically sealing the cell while incorporating a counter electrode separated by an ion-conductive membrane, which allows physical separation of catholyte and anolyte compartments. This feature is critical in electrocatalysis, where accurate quantification of gas and liquid products is essential. In our earlier work, we introduced two gastight RCE cells with well-characterized hydrodynamics (Figure 1A,B), a working electrode cylinder area of 3 cm^2 (fifteen times larger than that of a typical RDE), and detection limits in the micromolar and parts-per-million range for liquid and gas products, respectively.[20] The first-generation gastight RCE (RCE-1) shown in Figure 1A was restricted to a low maximum current density (−7.5 mA/cm^2 in 0.1 M $KHCO_3$, Figure 1D) because the distance between the working (WE) and counter (CE) electrode was very long

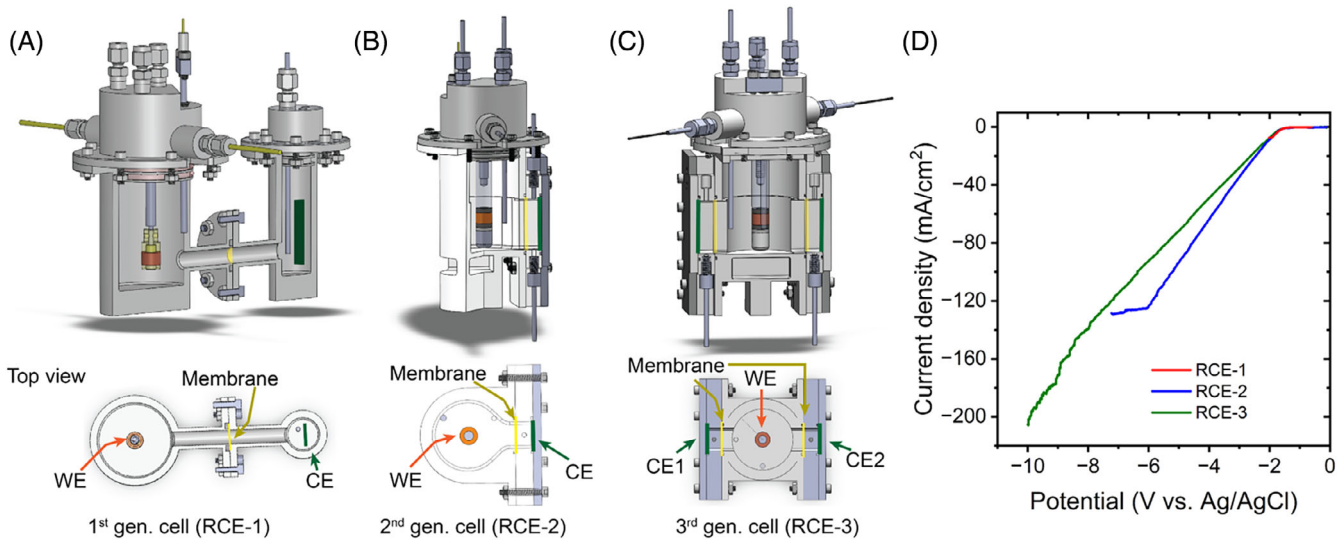

FIGURE 1 Schematics and current capacity comparison of three generations of the gastight RCE cell. (A) First-generation RCE cell (RCE-1) with an H-cell design. (B) Second-generation RCE cell (RCE-2) with a flat counter electrode compressively attached to one side of the cell. The distance between the working and counter electrode is shorter, and the cross-sectional area of the ion-conductive membrane separating the two cell compartments is larger compared to RCE-1. (C) Third-generation RCE cell (RCE-3), featuring two flat counter electrodes placed symmetrically on opposite sides of the cylinder. In all the RCE cells, the cylinder electrode has a diameter of 12 mm and an electrode active area of 3 cm^2. (D) Current-potential response measured on an electropolished copper cylinder working electrode in each of the three generations of the RCE cell using Pt foils as counter electrode and a Ag/AgCl reference electrode in 0.1 M $KHCO_3$. No iR correction is applied. Measured solution resistances between the working and reference electrode were respectively 9.5 Ω, 9.3 Ω, and 12.3 Ω for the RCE-1, RCE-2, and RCE-3 cells. Here, shortening the distance between the working and counter electrodes, increasing the cross-sectional area of the ion-conductive membrane, and doubling the counter electrode area increase the maximum current capacity achievable in the cell. The maximum potential that can be applied between the reference and the cylinder electrode is 10 V.

and the cross-section area of the membrane separating the two electrode compartments was very small.[20] The second-generation RCE cell design (RCE-2) shown in Figure 1B, addressed these limitations by bringing the two electrodes closer together and by increasing the cross-sectional area of the membrane separating the two compartments. In the RCE-2, the counter electrode was a flat metal foil with an active area of 6 cm^2 compressively attached to one side of the cell. This new design increased the maximum current density achievable to over -125 mA/cm^2 in 0.1 M $KHCO_3$ (Figure 1D). The RCE-2 cell thus enabled systematic studies of intrinsic kinetics decoupled from mass transport[20] across a wide range of electrocatalytic reactions at different current densities, and this in turn allowed a more technical analysis in dimensionless terms of multi-electron and multi-product electrocatalytic reactions such as the electrochemical oxidation of methane[21] and reactive CO_2 capture (RCC).[22]

One of the major advantages of the RCE-2 cell in the study of electrocatalytic systems is that it provides consistent hydrodynamics at the electrode surface regardless of the chemistry under study. This is because all the momentum transfer to the fluid occurs within a few hundred micrometers from the electrode, where the viscous sublayer thickness is well-defined all around the cylinder.[23] The RCE-2 design was used to determine an empirical dimensionless relation that universally linked cell hydrodynamics to mass film transfer coefficients for any reaction substrate, intermediate, and product with 20% accuracy.[20] Although mass transport is well-defined, multi-physics simulations that include electric potentials described below reveal that the RCE-2 design suffers from distortions of the electric field and current distribution (Figures S1–S5 in Supporting Information), particularly under conditions of low electrolyte conductivity and high current densities. The difference in potential drop between the various points on the surface of the cylinder electrode and the counter electrode on one side of the cell can be on the order of hundreds of millivolts for typical current densities used in electrocatalysis, and complicates the study of electrode kinetics, particularly in low conductivity electrolytes (Figure 2). To address these limitations, we have developed a third-generation gastight RCE cell (RCE-3) that introduced two flat counter electrodes placed symmetrically on opposite sides of the cylinder with a total counter electrode area of 12 cm^2 (Figure 1C). This modification doubles the counter electrode area relative to the RCE-2, reduces current density at the counter electrode surfaces, and improves the uniformity of the electric field.

In this work, we validate the design of the RCE-3 cell, characterize its hydrodynamics, and compare them with those of earlier RCE cells. The electric field symmetry is experimentally evaluated using CO_2 reduction as a probe reaction. The results demonstrate that the RCE-3 preserves the well-defined hydrodynamics of earlier RCE designs while greatly reducing electric field distortions, particularly in non-aqueous electrolytes. In addition to the new cell design, we introduce the use of a bipotentiostat as a novel means to control current densities on the two counter electrodes and maintain a uniform electric field. The RCE-3 cell thus allows for more reliable extraction of electrode kinetic parameters across a wide range of electrolyte conductivities and contributes to a more systematic characterization of catalysts for the future scale-up of electrocatalytic technologies.

2 | RESULTS AND DISCUSSION

2.1 | Electric field distortions in RCE-2 and design of RCE-3

The motivation to redesign the RCE-2 cell emerges from the growing interest in characterizing electrocatalytic systems in non-aqueous electrolytes. The RCE-2 cell consists of a main working electrode compartment and a smaller counter electrode compartment attached on one side of the cell, as shown in Figure 2A. Figure 2C,D shows the result of a multi-physics simulation when a potential of -5 V against the counter electrode was applied on the cylinder electrode. The model development for the multi-physics simulation is detailed in the Supporting Information. Notably, the effective electrolyte potential at the cylinder surface can vary by more than a hundred millivolts between the side facing the counter electrode and the side away from it (Figure 2D) when the current density is on the order of 10 mA/cm^2. Multi-physics simulations on the RCE surface for the hydrogen evolution reaction in the RCE-2 cell (Supporting Information) show that the effective electrolyte potential on different points over the surface of the cylinder can differ by 15 mV at 1 mA/cm^2 (Figure S5) in this cell configuration when using 0.1 M $KClO_4$ as the supporting electrolyte. These findings are not necessarily new or unexpected,[14] since this has been extensively studied via numerical simulations in both a RCE system[24] and a rotating cylinder Hull system,[25] and yet underscore the need for a redesigned RCE geometry that could maintain the advantages of a gastight configuration while ensuring symmetric fields and reliable kinetic measurements. Field distortions are expected to be particularly acute in non-aqueous low conductivity electrolytes, where ohmic losses can significantly bias apparent electrocatalyst kinetics. Details on how these distortions relate to the classic framework of primary, secondary, and tertiary current distribution are provided in the Supporting Information, and a longer discussion is avoided here for brevity. Numerical simulation studies of rotating cylinder electrode cells have previously shown that asymmetric flat-plate counter-electrode configurations lead to non-uniform primary current distributions, whereas symmetric or concentric counter-electrode geometries substantially restore electric field uniformity, with these effects becoming increasingly pronounced at higher current densities and lower electrolyte conductivity.[26] Importantly, these simulations further demonstrate that secondary and tertiary current distributions on the rotating cylinder approach uniformity when symmetric counter-electrode geometries are employed.

Inspired by previous work in improving current distributions on rotating cylinder electrodes,[26] we introduced two flat counter electrodes placed symmetrically on opposite sides of the cylinder in the RCE-3 cell design (Figure 1C). The cell cap was also redesigned so that the reference electrode could be positioned equidistantly from both counter electrodes. Although a concentric counter electrode

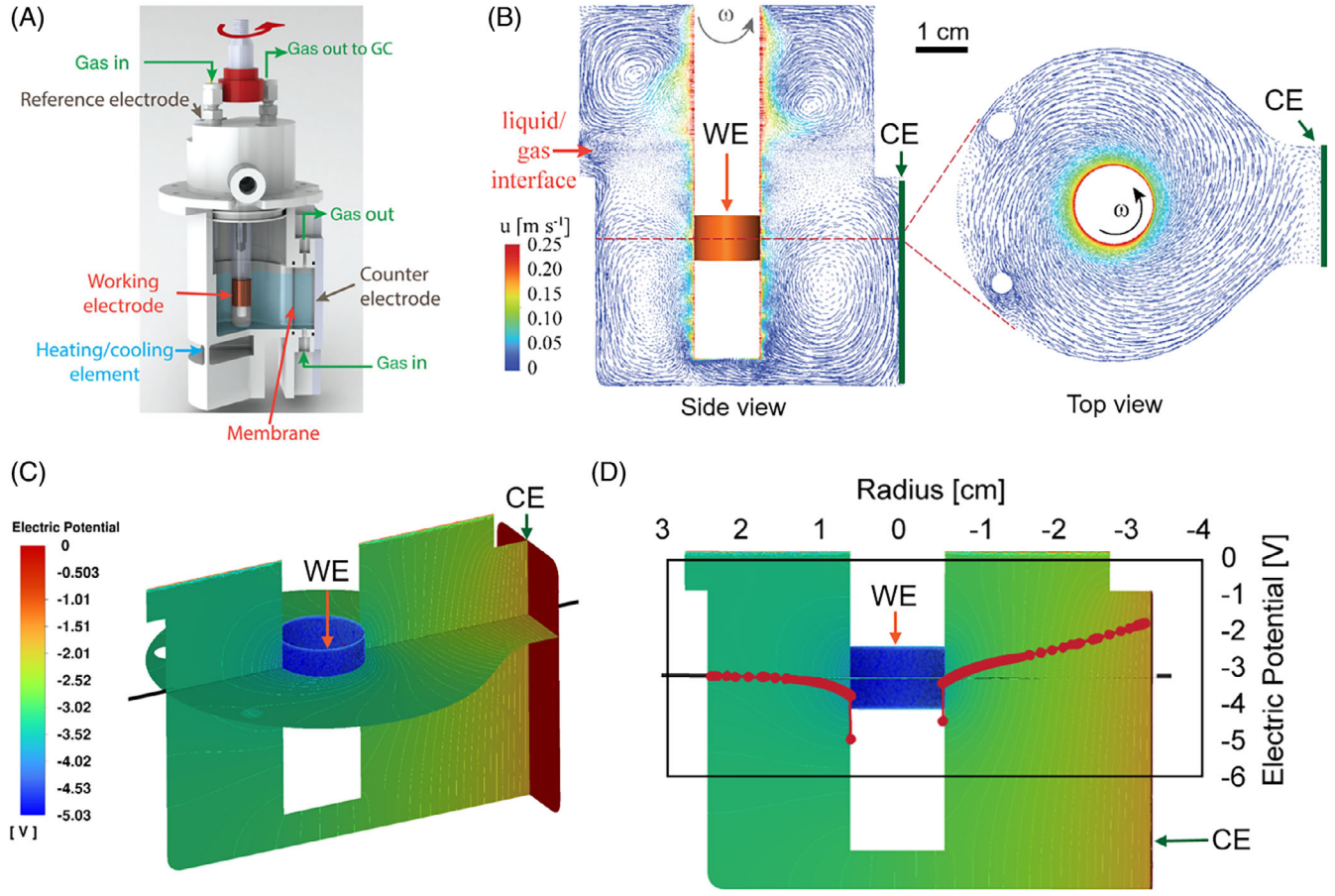

FIGURE 2 (A) Schematic of the gastight RCE-2 cell developed in our earlier work,[20] showing the hermetically sealed design and physical separation of catholyte and anolyte compartments by an ion-conductive membrane. (B) Cross-section and top view of the fluid velocity profiles in the RCE cell at 400 rpm,[23] which remains consistent across different electrocatalytic transformations. The fluid velocity profile shows the concentration of the momentum transfer to the liquid in a very thin layer around the cylinder electrode. (C) Results of multiphysics simulations of mass and charge transport, illustrating distortions in the electric field in the RCE-2 cell design, under conditions of low electrolyte conductivity and high current density for an applied voltage of 5 V between the working and counter electrode. (D) Electric potential as a function of position along the radial direction of the cylinder electrode for the RCE-2 cell under conditions of low electrolyte conductivity and high current density in (C). The potential difference between the surface of the cylinder electrode facing the counter electrode and the surface facing away from it can be over a couple of hundred millivolts.

surrounding the cylinder would provide the most uniform field,[27] incorporating a cylindrical ion-exchange membrane poses engineering challenges in a gastight configuration.[28] The use of two flat electrodes, therefore, represents a practical compromise that increases field symmetry while maintaining compatibility with quantitative product detection.

The ratio of working to counter electrode areas is critical in determining the maximum current density that can be sustained. Larger counter electrode areas lower current density at the counters, reduce overpotentials, and minimize parasitic reactions. In the RCE-3 cell, the total counter electrode area is twice that of the RCE-2 cell. As shown in Figure 1D, this modification allows the RCE-3 cell to maintain stable current densities that exceed −200 mA/cm^2 in 0.1 M $KHCO_3$ when using a Cu cylinder working electrode and Pt foil counter electrodes, compared to −125 mA/cm^2 in the RCE-2 cell under identical conditions.

This progression illustrates a systematic evolution of gastight RCE cell designs. The RCE-1 cell was limited by resistance associated with membrane and compartment geometry, the RCE-2 cell was limited by counter electrode kinetics and area, and the RCE-3 cell, by design, now achieves higher current densities with improved symmetry of the electric field, while preserving the gastight architecture required for quantitative product analysis. In the following section, we evaluate whether these modifications alter the well-defined hydrodynamic characteristics of the RCE geometry.

2.2 | Characterization of hydrodynamics

To verify that the modifications introduced in the RCE-3 did not alter the well-defined transport properties of the RCE geometry

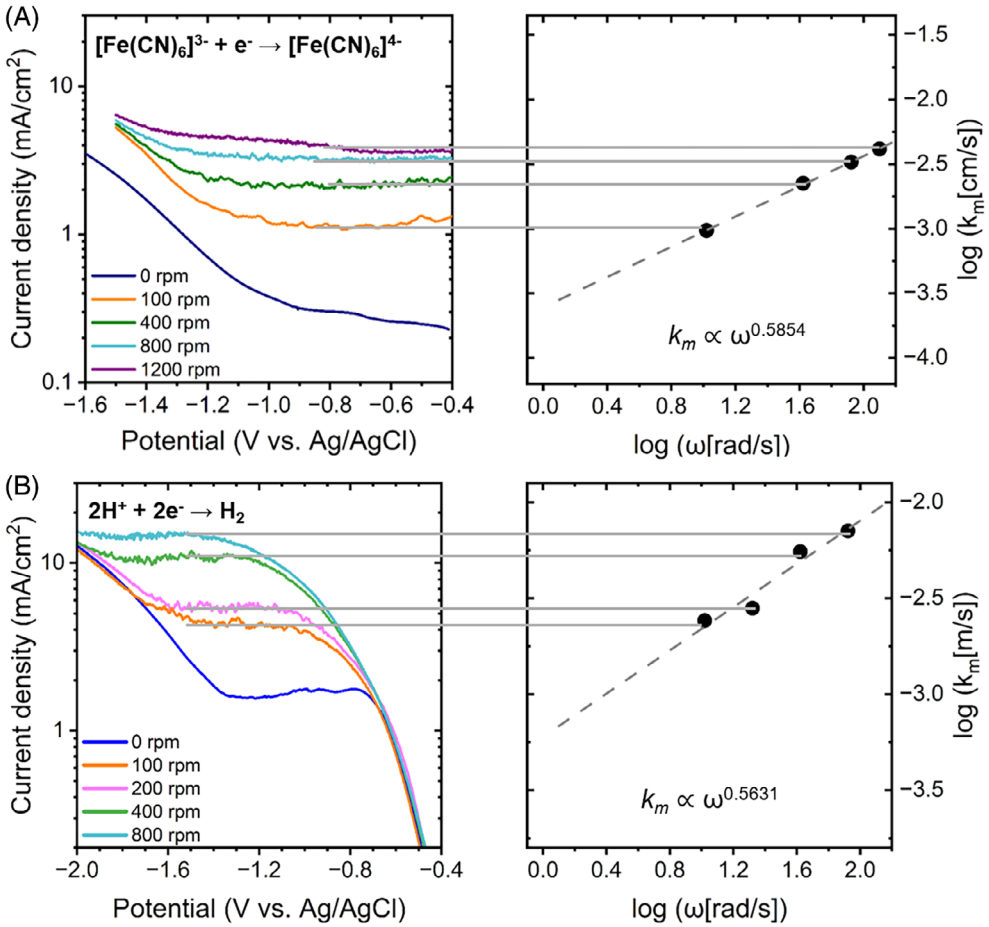

FIGURE 3 Determination of the mass transfer coefficient (k_m), in the gastight RCE-3 cell from limiting current measurements during the electrochemical reduction of (A) ferricyanide and (B) protons. Currents were measured on a sputtered silver rotating cylinder electrode as a function of rotation speed in 0.1 M $KClO_4$ containing 10 mM of the respective reactants $K_3[Fe(CN)_6]$ and $HClO_4$.

itself, we characterized mass transport using the electrochemical reduction of ferricyanide (Equation 1) and protons (Equation 2) as probe reactions. These systems were chosen because their kinetics are fast enough that the current at high overpotentials becomes solely limited by mass transport (Figure 3). In this regime, the limiting current reflects the convective–diffusive transport of species to the electrode surface.

$$[Fe(CN)_6]^{3-} + e^- \rightleftharpoons [Fe(CN)_6]^{4-} \quad (1)$$

$$2H^+ + 2e^- \rightleftharpoons H_2 \quad (2)$$

The mass transfer coefficient (k_m) was obtained from the limiting current density (j_{lim}) according to:

$$j_{lim} = \frac{i_{lim}}{A} = zFC_{i,b}k_m \quad (3)$$

where i_{lim} is the limiting current, A the electrode area, z the number of electrons transferred, F Faraday's constant, and $C_{i,b}$ the bulk concentration of electroactive species.

To standardize mass transport analysis across different reactants, dimensionless groups were introduced. The Reynolds number (Re) characterizes the ratio of inertial to viscous forces:

$$Re_{RCE} = \frac{U_{cyl}d_{cyl}\rho}{\mu} \quad (4)$$

where U_{cyl} is the peripheral velocity of the cylinder, d_{cyl} its diameter, ρ the fluid density, and μ the viscosity.

The Schmidt number (Sc) compares the kinetic viscosity of the fluid to the molecular diffusivity of the electroactive species:

$$Sc = \frac{\mu}{D\rho} \quad (5)$$

and provides a measure of the relative rates of momentum and mass transport by diffusion in a fluid. The Schmidt number simplifies the understanding of how these relative rates are affected by changes in the temperature of the system, without the need to treat these variables explicitly.

Finally, the Sherwood number (Sh) represents the ratio of convective to diffusive transport:

$$Sh_{RCE} = \frac{k_m}{D/d_{cyl}} \quad (6)$$

For the RCE system, an empirical correlation[14] establishes the relation between these dimensionless numbers:

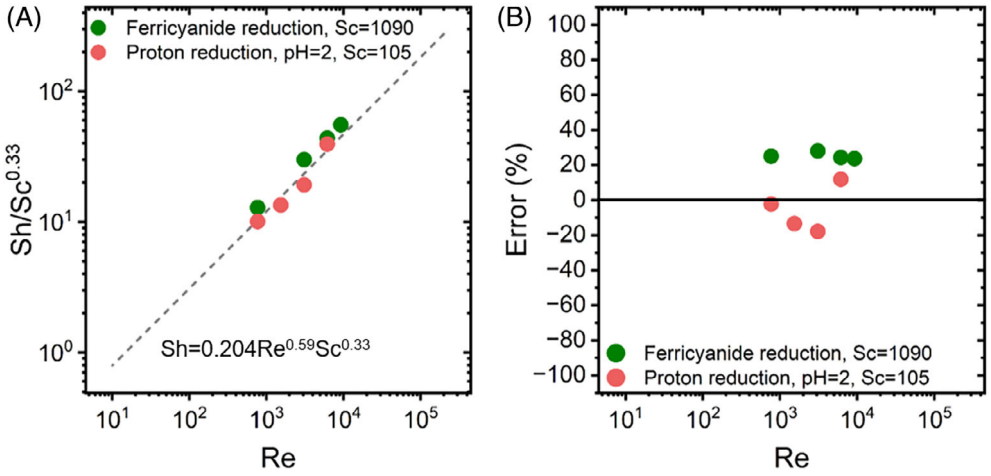

FIGURE 4 Dimensionless analysis of hydrodynamics in the RCE-3 cell. (A) Correlation between the Sherwood, Reynolds, and Schmidt numbers for ferrocyanide and proton reduction experiments in Figure 3. Experimental results show that the relation between mass-transport to the cylinder electrode and the hydrodynamics in the cell for the RCE-3 is the same empirical correlation as that in the RCE-2 cell ($Sh = 0.204Re^{0.59}Sc^{0.33}$), confirming that the addition of a second counter electrode does not alter the hydrodynamics of the system and the mass transport of species to the surface of the cylinder electrode. (B) Relative error between measured and predicted Sh values using the experimental correlation of the RCE-2 cell in Equation (7).

$$Sh_{RCE} = 0.204Re_{RCE}^{0.59}Sc^{0.33} \quad (7)$$

The relation between rotation rate and mass transport for both the RCE-2 and RCE-3 collapse onto the same Sherwood–Reynolds–Schmidt relation in Equation (7)[20] (Figure 4A), confirming that the addition of the second counter electrode does not alter the hydrodynamics. The relative error between the measured and predicted Sherwood numbers (Figure 4B) is below or around 20%, consistent with the variability previously reported for the RCE-2 cell described and characterized by Jang et al.[20]

The exponent of 0.59 for the Reynolds number suggests that eddy-driven mixing dominates mass transport in the turbulent boundary layer at the high-Re regime in the RCE cells. In this regime, the viscous sublayer adjacent to the electrode shrinks to just a few micrometers and is still disrupted by eddies formed in the buffer layer. This thin viscous sublayer is uniform around the cylinder surface area of 3 cm^2, and guarantees that the reactants and products enter and exit the electrode surface at all points, eliminating concentration gradients along tangential and azimuthal directions of the electrode.[23] By contrast, in the RDE system, the 0.5 Reynolds exponent reflects transport dominated by molecular diffusion alone in the viscous sublayer and the dragging of reactants and intermediates along the radial direction of the disk.[6] These concentration gradients become more significant with larger electrode areas, and this is why the RDE is limited to an electrode surface area of just around 0.2 cm^2. This distinction highlights the fundamentally different transport regimes of RCE and RDE geometries.[14]

Together, these results demonstrate that the RCE-3 cell maintains the same well-defined transport behavior as previous RCE designs, ensuring that the improved counter electrode symmetry does not compromise the hydrodynamic advantages of the cylinder geometry.

2.3 | Effects of uniform electric field on electrochemical CO_2R product distribution

The impact of counter electrode symmetry on electrocatalytic measurements was evaluated during electrochemical reduction of CO_2, where it is well known that hydrogen, CO, formate, and C_1 and C_2 hydrocarbon and oxygenates are the major products on Cu electrodes. Figure 5 shows the different configurations used in this work to connect the cylinder and the two Pt foils as working or counter electrodes. Electrolysis was performed in 0.1 M $KHCO_3$ at −1.40 V vs. SHE using an electropolished copper cylinder as the working electrode, and two Pt foils connected to the same potentiostat lead as the counter electrode. This is schematically shown in Figure 5C, where the positioning of the two counter electrodes and the reference electrode is shown relative to the working electrode. Gaseous products were quantified by online gas chromatography, while the liquid product (formate) was quantified by post-electrolysis ^1H NMR. Notably, the concentration of formate differed by a factor of 4.7 between the left (CEL) and right (CER) anolyte compartments (Figure 6A). The crossover of the product formate through the anion exchange membrane is both current-dependent and potential-dependent, since formate is a negatively charged compound.[29] The difference in concentration of formate between the two counter electrode compartments reflects an asymmetric secondary current distribution between the two electrodes, with current being higher at the counter electrode on the left of the cell (CEL). It must be noted that still most of the formate remains in the working electrode chamber in the center of the cell, where the concentration of formate is similar, but the volume of electrolyte is larger.

This asymmetry in concentration of the formate in the two counter electrode chambers indicated that having two counter electrodes

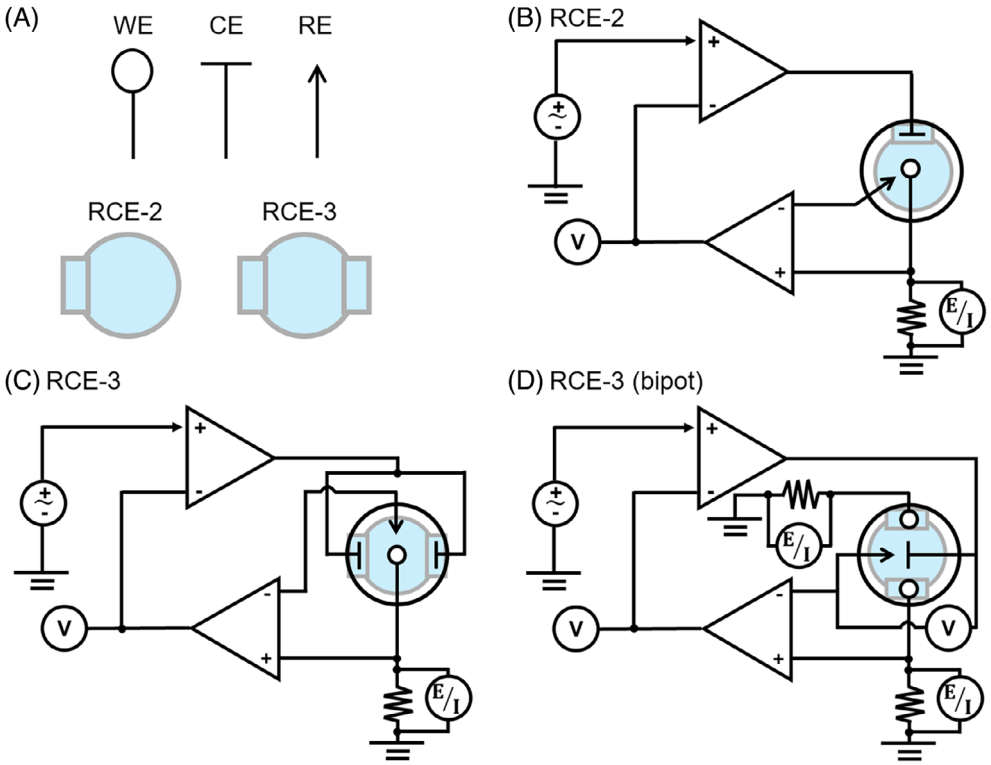

FIGURE 5 Electrical configurations of the RCE-2 and RCE-3 cells. (A) Symbol key for working (WE), counter (CE), and reference (RE) electrodes. (B) RCE-2 cell, consisting of a cylinder working electrode and a single counter electrode. (C) RCE-3 cell operated in the conventional configuration, with the cylinder as the working electrode and two Pt foils connected in parallel as counter electrodes. The reference electrode is positioned at the midplane to approximate electrochemical centering. (D) RCE-3 cell operated with a bipotentiostat, in which the two Pt foils are controlled independently as working electrodes, while the cylinder in the center of the cell is the counter electrode. The bipotentiostat ensures symmetric potential shifts at both Pt electrodes relative to the cylinder, eliminating field distortions.

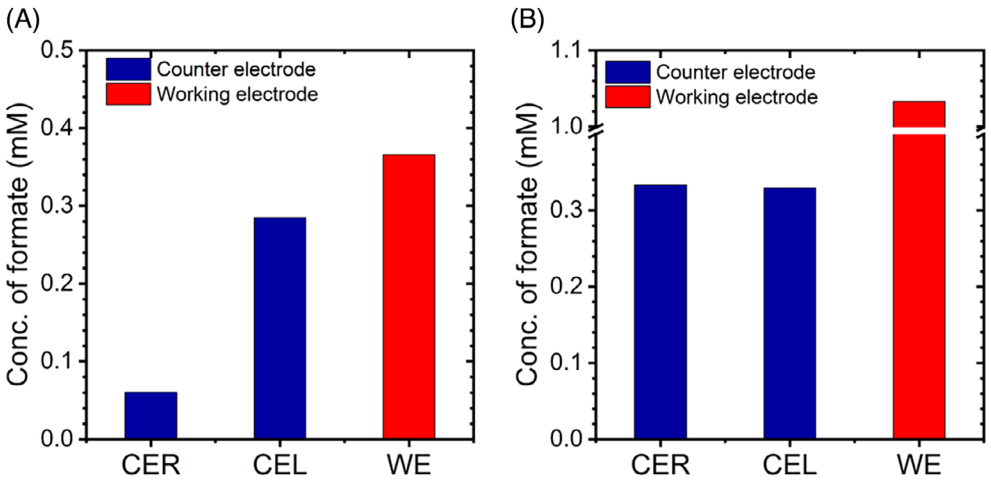

FIGURE 6 Quantification of formate crossover in the RCE-3 cell during aqueous CO_2 reduction in 0.1 M $KHCO_3$ at 100 rpm and −1.40 V vs. SHE. Here, an electropolished Cu cylinder is used as the working electrode, and Pt foils as counter electrodes. Formate concentrations measured in the left (CEL) and right (CER) anolyte compartments (A) before and (B) after making the activity of the two Pt electrodes and resistance of the membranes the same. Asymmetric formate distribution in (A) shows that geometric symmetry alone is not sufficient and that the electrode activity and membrane resistance also matter. The experiment in (B) is carried out in a bipotentiostat mode, schematically shown in Figure 5D.

of identical geometric area located more or less equidistant from the cylinder was not sufficient to ensure field uniformity: The activity of each counter electrode must also be identical. To verify this, cyclic voltammetry was performed separately on each of the two Pt foils by connecting them as the working electrode. The response of each Pt foil (labeled as right or left depending on their position relative to the

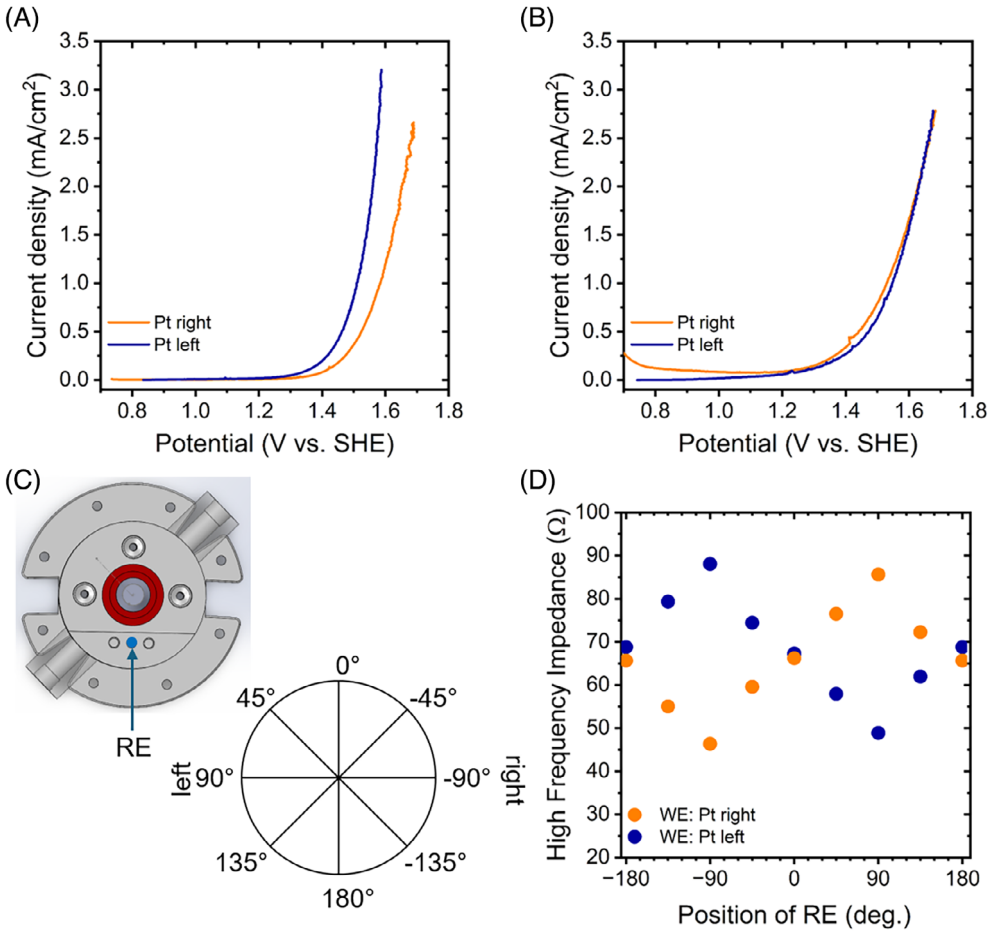

FIGURE 7 Evaluation of Pt counter electrode activity and membrane resistance in the RCE-3 cell using 0.1 M $KHCO_3$ as electrolyte. (A) Cyclic voltammetry of the original Pt foils shows non-overlapping current–potential curves, confirming unequal activities of the two electrodes. (B) Replacement with new Pt foils and membranes yields overlapping CVs, demonstrating matched activities that are required for field symmetry. (C) Schematic of the cap showing reference electrode positions used for impedance testing. (D) Change in high-frequency impedance response as a function of reference electrode (RE) position. Both membranes have comparable resistance.

Cu cylinder) is shown in Figure 7A. The original foils exhibited distinct current–potential curves, confirming unequal activities. The Pt electrode on the left side of the cell was more active (Figure 7A), and thus more of the anodic current was distributed to this electrode. This explains the higher concentration of formate in the left anolyte compartment in Figure 6A, demonstrating that formate concentration is a proxy for current distribution in this specific experiment. When the two Pt foils are replaced with new foils and new membranes are used, the current–potential curves for the two anodes overlapped (Figure 7B), highlighting that electrode activity matching is critical for achieving a symmetric electric field and current distribution.

Electrode activity alone, however, could not fully account for the observed asymmetry. The membrane resistance also contributes significantly to the total resistance between each counter electrode and the reference electrode located in the middle compartment. To assess this, electrochemical impedance spectroscopy (EIS) was conducted with the two Pt foils on each side of the cell connected as working and counter electrodes, and with the reference electrode sitting in the middle compartment between the two cell membranes. Impedance measurements were taken as the reference electrode position was rotated in 45° increments (Figure 7C,D) for the two cases where each Pt foil was connected as the working electrode. The results demonstrated that the pair of membranes had comparable resistance, but slight differences ($\leq$ 1 Ω) remained between each Pt foil and the reference electrode. These residual differences can distort the secondary current distribution even after centering the reference electrode.

To overcome this limitation, we implemented a bipotentiostat configuration (bipot) in which both Pt foils were independently controlled as working electrodes (WE1 and WE2), while the Cu cylinder served as the counter electrode (Figure 5D). This arrangement ensured that equal currents were independently enforced at both Pt foils, resulting in a uniform electric field distribution on both sides of the Cu cylinder. It should be noted that this configuration does not change the electrode of interest; the focus remains on CO_2reduction at the copper cylinder. Another approach could be to add large resistors between the counter electrodes and the counter electrode connector. Unlike the bipotentiostat, this method requires a higher applied voltage and lacks precise control over the current supplied to each counter electrode.

Using the RCE-3 (bipot) operation, we observed that the formate concentration became identical in both anolyte compartments (Figure 6B), confirming that the bipotentiostat successfully restored symmetry to the electric field.

Together, these experiments demonstrate that the apparent kinetics and product distributions measured in the RCE-3 could depend sensitively on counter electrode symmetry. Reliable kinetic analysis requires not only geometric balance but also matched electrode activity, balanced membrane resistance, and appropriate

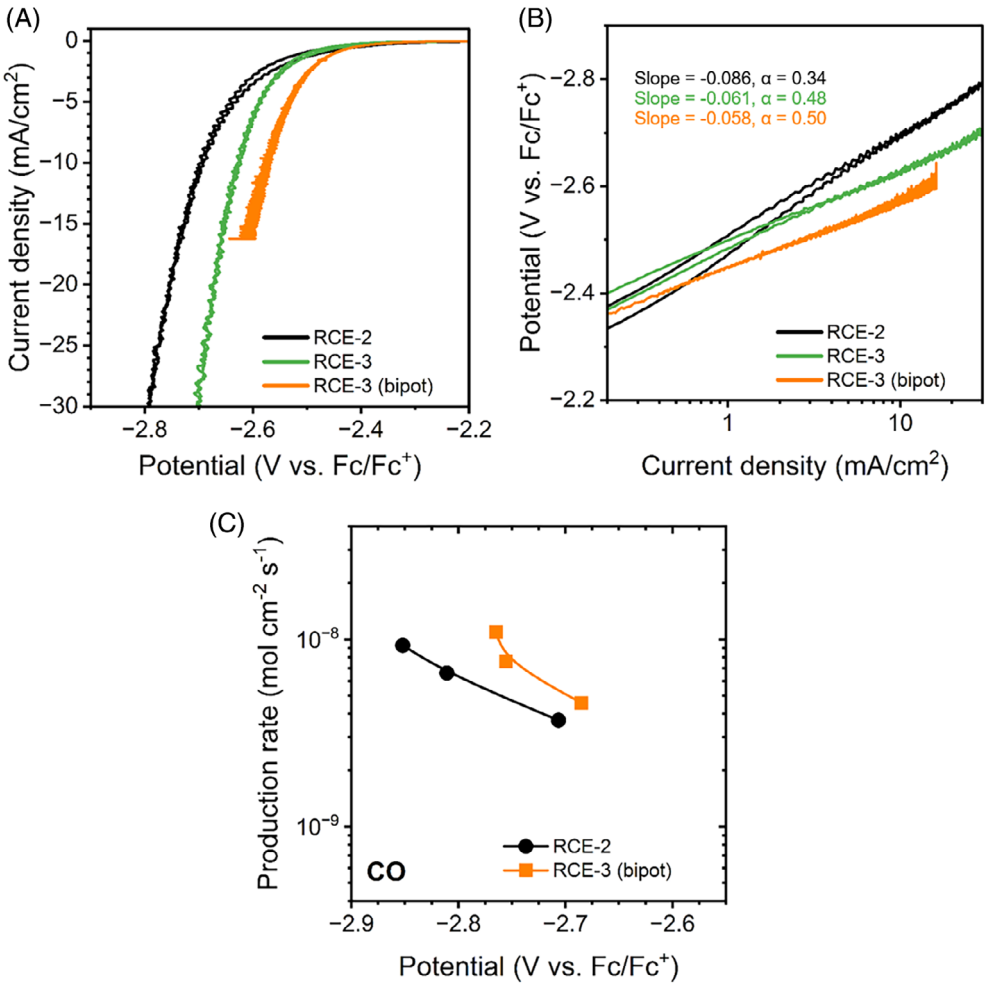

FIGURE 8 Performance of the RCE-3 cell in non-aqueous CO_2 reduction. (A) Cyclic voltammetry of silver cylinder electrodes in 0.1 M $TBAPF_6$ in acetonitrile at 100 rpm comparing the RCE-2 cell, the RCE-3 cell operated conventionally, and the RCE-3 cell operated with a bipotentiostat. The RCE-3 cell exhibits lower overpotentials at fixed current densities, with the bipotentiostat configuration providing the best performance. (B) Tafel plots extracted from the same experiments show that only the RCE-2 cell deviates from the expected transfer coefficient of $\alpha \approx 0.5$, while both RCE-3 cell configurations approach $\alpha \approx 0.5$. (C) Production rate of CO in non-aqueous CO_2 reduction in 0.1 M $TBAPF_6$ in acetonitrile on a bulk silver rotating cylinder electrode at 100 rpm.

potential control. The bipotentiostat configuration provides a practical means to achieve these conditions, eliminating asymmetries that would otherwise bias product quantification. Supporting Information Figure S6 shows that the product distribution as a function of potential in aqueous electrolytes for the RCE-2 and RCE-3 cells remains largely unchanged by the addition of the second counter electrode, likely due to the high conductivity of the aqueous bicarbonate electrolyte. This is in agreement with the initial multiphysics simulations that predicted a difference in surface overpotentials in the range of 15 millivolts for current densities of the order of 1 mA/cm^2 for the 0.1M $KClO_4$electrolyte, which has a similar conductivity to the 0.1M $KHCO_3$ electrolyte. Although the difference in surface overpotentials in the RCE-2 cell is not negligible, it does not affect the study of CO_2 reduction in the bicarbonate electrolyte when the potential window studied is greater than a few hundred millivolts and the current densities are in the range of 1 to 10 mA/cm^2.

2.4 | Non-aqueous CO_2R

Field distortions are expected to be more severe in non-aqueous systems due to the low ionic conductivity of organic electrolytes. To evaluate the performance of the RCE-3 under these conditions, we carried out CO_2 reduction in 0.1 M $TBAPF_6$ in acetonitrile using a silver cylinder as the cathode electrode.

Three configurations of the RCE cells and their operation were compared using cyclic voltammetry (CV) (Figure 8A). The difference in the absolute current density value at an applied potential is a function of the catalyst synthesis and the number of active sites on the surface as each experiment used a new electrode; however, the observed Tafel slope and the charge transfer coefficient depend on the electrochemical reduction mechanism and the electric field distribution. Despite the current densities being similar at low overpotential, the charge transfer coefficient for the silver electrode tested in the RCE-2 cell is smaller than that observed in the RCE-3 cell (Figure 8B). The use of one or two counter electrodes around the rotating cylinder electrode is already enough to affect the observed charge transfer coefficient. These results confirm that field asymmetries, which are amplified in low-conductivity electrolytes, can be mitigated by the symmetric counter electrode configuration and bipotentiostat control.

Tafel analysis is often invoked to discuss reaction mechanism and in recent years, it has been finally acknowledged that the cell geometry and the cell hydrodynamics have a large impact on the Tafel slope measured.[30] We have shown here that the cell hydrodynamics are the

same in the RCE-2 and the RCE-3 cell, and the experiments carried out in the non-aqueous electrolytes provided further evidence that the field symmetry also affects the Tafel slope observed. In the RCE-2 cell, the apparent transfer coefficient (α) deviated substantially from the expected value of 0.5 for CO_2 reduction in aprotic organic electrolytes. In contrast, both configurations of the RCE-3 yielded $\alpha \approx 0.5$, consistent with theoretical expectations[31] and confirming that the new design minimizes measurement artifacts caused by electric field distortions (Figure 8B).

Constant current electrolysis was also performed in the RCE-2 and RCE-3 cells to see how the electric field could affect product distribution in non-aqueous CO_2 reduction. The experiments were conducted using a silver cylinder electrode at fixed currents of -1, -1.67, and -2.3 mA/cm^2. Figure 8C shows the production rate of CO as a function of potential. The potential here is corrected for the resistance of the electrolyte between the silver cylinder and the reference electrode. In agreement with the cyclic voltammograms in Figure 8A, the overpotential on silver for each current was lower in the RCE-3 cell operated in the bipotentiostat mode compared to the RCE-2 cell. Nevertheless, the only product observed is CO, indicating that for this specific system, the Faradaic efficiency is not changed, but the current-potential response is affected by the distortion of the electric field. As the applied current increases, the difference in the measured overpotential becomes more significant in the non-aqueous electrolytes compared to the aqueous systems for the CO_2 reduction in the RCE cells (Figure S7). The use of the RCE-3 cell will be beneficial for the study of CO_2 reduction using non-aqueous systems or ionic liquids under well-defined mass transport conditions.

3 | CONCLUSION

In this work, we modified our previously reported RCE-2 cell to include two flat counter electrodes placed symmetrically on opposite sides of the cylinder. This RCE-3 cell doubles the counter electrode area compared to the RCE-2 design, resulting in reduced counter electrode overpotentials and a higher maximum achievable current density.

Hydrodynamic characterization confirmed that the new RCE-3 cell follows the same Sherwood–Reynolds–Schmidt correlation as the RCE-2 cell, demonstrating that the addition of a second counter electrode does not alter the well-defined transport properties of the RCE geometry. Instead, the primary effect of the new design is to improve the uniformity of the electric field at the cylinder electrode surface.

Electrochemical CO_2 reduction experiments highlighted the importance of counter electrode symmetry. When the Pt foils had unequal activity, significant asymmetry was observed in the distribution of formate between the two anolyte compartments. After replacing the foils and using a bipotentiostat configuration, the activities were balanced, and the product distribution became symmetric. These results show that achieving reliable kinetic parameters with the RCE-3 cell requires not only geometric symmetry but also matched electrode activity, balanced membrane resistance, and appropriate potential control.

These results establish the RCE-3 cell as a robust platform for studying electrocatalysis under conditions where ohmic losses and field distortions are significant. By enabling accurate kinetic measurements while maintaining gastight operation for quantitative product detection, the RCE-3 cell provides a practical and scalable design for probing intrinsic electrocatalytic behavior in both conventional and low-conductivity electrolytes.

AUTHOR CONTRIBUTIONS

Momoko Ishida: Data curation (lead); formal analysis (equal); investigation (equal); methodology (equal); software (equal); validation (equal); visualization (equal); writing – original draft (equal); writing – review and editing (equal). **Tyler Seung Hun Kwak:** data curation (supporting); formal analysis (supporting); investigation (supporting); methodology (supporting); writing – original draft (supporting); writing – review and editing (supporting). **Derek Richard:** conceptualization (equal); simulation (equal). **Saudagar Dongare:** methodology (equal); writing – review and editing (equal). **Burcu Gurkan:** methodology (equal); writing – review and editing (equal). **Panagiotis D. Christofides:** conceptualization (equal); simulation (equal). **Carlos G. Morales-Guio:** conceptualization (lead); simulation (lead); cell design (lead); data curation (lead); formal analysis (lead); funding acquisition (lead); investigation (lead); methodology (lead); project administration (lead); resource (lead); software (lead); supervision (lead); validation (lead); visualization (lead); writing – original draft (lead); writing – review and editing (lead). Carlos Gilberto Morales-Guio conceived the idea and supervised the work.

ACKNOWLEDGMENTS

This work was supported as part of the Center for Closing the Carbon Cycle, an Energy Frontier Research Center funded by the U.S. Department of Energy, Office of Science, Basic Energy Sciences under Award Number DE-SC0023427 and the National Science Foundation through the CAREER award CBET-2339693.

CONFLICT OF INTEREST STATEMENT

The authors declare no conflict of interest.

FUNDING INFORMATION

This work was supported by the U.S. Department of Energy (DE-SC0023427) and the National Science Foundation (CBET-2339693).

DATA AVAILABILITY STATEMENT

The data that support the findings of this study and cell schematics are available from the corresponding author upon reasonable request. All experimental details are provided in the Supporting Information. All product quantification measurements and potential-current response of the system are provided in the Figures of this manuscript.

ORCID

Burcu Gurkan https://orcid.org/0000-0003-4886-3350
Panagiotis D. Christofides https://orcid.org/0000-0002-8772-4348
Carlos G. Morales-Guio https://orcid.org/0000-0002-5840-5591

REFERENCES

1. Perkin FM. A simple form of rotating electrode for electrochemical analysis. *Trans Faraday Soc*. 1906;2:91-93.
2. Millet P. Electric potential distribution in an electrochemical cell. *J Chem Educ*. 1996;73:956.
3. Bard AJ, Faulkner LR, White HS. *Electrochemical Methods: Fundamentals and Applications*. John Wiley & Sons; 2022.
4. Lazaridis T, Stühmeier BM, Gasteiger HA, El-Sayed HA. Capabilities and limitations of rotating disk electrodes versus membrane electrode assemblies in the investigation of electrocatalysts. *Nat Catal*. 2022;5:363-373.
5. Newman J. Current distribution on a rotating disk below the limiting current. *J Electrochem Soc*. 1966;113:1235.
6. Marathe V, Newman J. Current distribution on a rotating disk electrode. *J Electrochem Soc*. 1969;116:1704.
7. Liang S, Altaf N, Huang L, Gao Y, Wang Q. Electrolytic cell design for electrochemical CO_2 reduction. *J CO2 Utiliz*. 2020;35:90-105.
8. Wu J, Sharma PP, Harris BH, Zhou X-D. Electrochemical reduction of carbon dioxide: IV dependence of the faradaic efficiency and current density on the microstructure and thickness of tin electrode. *J Power Sources*. 2014;258:189-194.
9. Weekes DM, Salvatore DA, Reyes A, Huang A, Berlinguette CP. Electrolytic CO_2 reduction in a flow cell. *Acc Chem Res*. 2018;51:910-918.
10. Simonson H, Klein WE, Henckel D, Verma S, Neyerlin K, Smith W. A. Direct measurement of electrochemical selectivity gradients over a 25 cm^2 copper gas diffusion electrode. *ACS Energy Letters*. 2023;8:3811-3819.
11. Vos RE, Kolmeijer KE, Jacobs TS, van der Stam W, Weckhuysen BM, Koper MT. How temperature affects the selectivity of the electrochemical CO_2 reduction on copper. *ACS Catal*. 2023;13:8080-8091.
12. Huang L, Gao G, Yang C, et al. Pressure dependence in aqueous-based electrochemical CO_2 reduction. *Nat Commun*. 2023;14:2958.
13. Nitopi S, Bertheussen E, Scott SB, et al. Progress and perspectives of electrochemical CO_2 reduction on copper in aqueous electrolyte. *Chem Rev*. 2019;119:7610-7672.
14. Newman J, Balsara NP. *Electrochemical Systems*. John Wiley & Sons; 2021.
15. Levich VG, Tobias CW. Physicochemical hydrodynamics. *J Electrochem Soc*. 1963;110:251C.
16. White R, Newman J. Simultaneous reactions on a rotating-disk electrode. *J Electroanal Chem Interfacial Electrochem*. 1977;82:173-186.
17. Gabe DR, Wilcox G, Gonzalez-Garcia J, Walsh F. The rotating cylinder electrode: its continued development and application. *J Appl Electrochem*. 1998;28:759-780.
18. Walsh F, Kear G, Nahle AH, Wharton J, Arenas L. The rotating cylinder electrode for studies of corrosion engineering and protection of metals—an illustrated review. *Corros Sci*. 2017;123:1-20.
19. Rivero E, Granados P, Rivera F, Cruz M, González I. Mass transfer modeling and simulation at a rotating cylinder electrode (RCE) reactor under turbulent flow for copper recovery. *Chem Eng Sci*. 2010;65:3042-3049.
20. Jang J, Rüscher M, Winzely M, Morales-Guio CG. Gastight rotating cylinder electrode: toward decoupling mass transport and intrinsic kinetics in electrocatalysis. *AIChE J*. 2022;68:e17605.
21. Shen K, Kumari S, Huang Y-C, Jang J, Sautet P, Morales-Guio CG. Electrochemical oxidation of methane to methanol on electrodeposited transition metal oxides. *J Am Chem Soc*. 2023;145:6927-6943.
22. Shen K, Cheng D, Reyes-Lopez E, Jang J, Sautet P, Morales-Guio CG. On the origin of carbon sources in the electrochemical upgrade of CO_2 from carbon capture solutions. *Joule*. 2023;7:1260-1276.
23. Richard D, Tom M, Jang J, Yun S, Christofides PD, Morales-Guio CG. Quantifying transport and electrocatalytic reaction processes in a gastight rotating cylinder electrode reactor via integration of computational fluid dynamics modeling and experiments. *Electrochim Acta*. 2023;440:141698.
24. Rosales M, Nava JL. Simulations of turbulent flow, mass transport, and tertiary current distribution on the cathode of a rotating cylinder electrode reactor in continuous operation mode during silver deposition. *J Electrochem Soc*. 2017;164:E3345-E3353.
25. Low C, Roberts E, Walsh F. Numerical simulation of the current, potential and concentration distributions along the cathode of a rotating cylinder Hull cell. *Electrochim Acta*. 2007;52:3831-3840.
26. Pérez T, Nava JL. Numerical simulation of the primary, secondary and tertiary current distributions on the cathode of a rotating cylinder electrode cell. Influence of using plates and a concentric cylinder as counter electrodes. *J Electroanal Chem*. 2014;719:106-112.
27. Stojak JL, Talbot JB. Investigation of electrocodeposition using a rotating cylinder electrode. *J Electrochem Soc*. 1999;146:4504-4513.
28. Walsh DR, Walsh FC. The rotating cylinder electrode: a review of development. *J Appl Electrochem*. 1983;13:3-21.
29. Krödel M, Carter BM, Rall D, Lohaus J, Wessling M, Miller DJ. Rational design of ion exchange membrane material properties limits the crossover of CO_2 reduction products in artificial photosynthesis devices. *ACS Appl Mater Interfaces*. 2020;12:12030-12042.
30. Watkins NB, Schiffer ZJ, Lai Y, et al. Hydrodynamics change Tafel slopes in electrochemical CO_2 reduction on copper. *ACS Energy Letters*. 2023;8:2185-2192.
31. Oppel N, Röse P, Heuser S, Prokein M, Apfel U-P, Krewer U. Unveiling the kinetics of CO_2 reduction in aprotic electrolyte: the critical role of adsorption. *Electrochim Acta*. 2024;490:144270.

SUPPORTING INFORMATION

Additional supporting information can be found online in the Supporting Information section at the end of this article.

How to cite this article: Ishida M, Kwak TSH, Richard DM, et al. Improved symmetry and current distribution in a gastight rotating cylinder electrode cell: Design and characterization. *AIChE J*. 2026;72(6):e70294. doi:10.1002/aic.70294